

1
2 Collisions of a light bullet with kinks and standing
3 breathers in the two-dimensional sine-Gordon equation

4 M. V. Pato*

5 *Dep. Física, Instituto Superior Técnico, Universidade Técnica de Lisboa*

6 P. Bicudo

7 *CFTP, Dep. Física, Instituto Superior Técnico, Av. Rovisco Pais, 1049-001 Lisboa, Portugal*

8 **Abstract**

9 The (2+1)-dimension Klein-Gordon generalised equation is numerically solved through the fi-
10 nite differences method. Only the sine-Gordon case is focused: kink and antikink solutions are
11 obtained in cartesian coordinates and evidence of interaction in kink-kink collision is looked for
12 in propagation velocity. Then the change of shape in light bullet solutions is quantified during
13 propagation and in head-on collision. Lastly, the robustness of light bullets is verified in head-on
14 collisions with kink, antikink, standing kink and standing breather. A 30°-collision between a
15 light bullet and a standing kink is simulated as well.

16 *Key words:* sine-Gordon equation, soliton, light bullet, kink, standing breather

17 *PACS:* 02.30.Jr, 02.70.Bf, 03.75.Lm, 42.81.Dp

18 **1. Introduction**

The Klein-Gordon generalised equation is written as

$$\nabla^2\phi - \frac{1}{c^2} \frac{\partial^2\phi}{\partial t^2} = F(\phi) \quad (1)$$

where F is an arbitrary function of ϕ . The well-known wave equation is obtained with
 $F(\phi) = 0$, while $F(\phi) = \left(\frac{mc}{\hbar}\right)^2 \phi$ leads to Klein-Gordon equation that describes a particle
of mass m and spin 0 in relativistic quantum mechanics. Both cases are linear and only

* Corresponding author.

Email addresses: migpato@gmail.com (M. V. Pato), bicudo@ist.utl.pt (P. Bicudo).

the latter is dispersive [1]. An important nonlinear case is characterised by $F(\phi) = \left(\frac{mc}{\hbar}\right)^2 \sin\phi$:

$$\nabla^2\phi - \frac{1}{c^2} \frac{\partial^2\phi}{\partial t^2} = \left(\frac{mc}{\hbar}\right)^2 \sin\phi \quad (2)$$

19 Equation (2) is the so-called sine-Gordon equation and allows soliton-like solutions.
 20 This type of solutions is increasingly important in the description of (at least partly)
 21 particle-like objects [2,3], which is easy to understand since solitons present very localised
 22 momentum and their shape consistency results in effective transportation of energy. For
 23 instance, the π -mesons are quark-antiquark bound states and some works (e.g. [3]) have
 24 been able to estimate pion mass values in good agreement with the experiment by de-
 25 scribing pions as breather-like solutions of sine-Gordon equation. In other words, the
 26 quark may be seen as a soliton (e.g. kink) and the antiquark as an antisoliton (e.g. anti-
 27 kink) so that π is a bound state of the two. Another example is the Josephson junction,
 28 where the phase difference between the electronic densities of the superconductors may
 29 be modeled by sine-Gordon equation which previews the vortex dynamics in type II su-
 30 perconductors [4,5]. The sine-Gordon equation finds also application in classical systems
 31 such as coupled pendula [6] and, finally, light bullet solutions may be identified with
 32 optical pulses propagating in different media [7,8].

33 In this paper, section 2 briefly describes the numerical method used, while section 3
 34 presents the results of the simulations and is organised as follows. In 3.1 the propagation
 35 and collision of kink-like solitons is analysed and in 3.2 an analogous study is performed
 36 for light bullet solutions. Section 3.3 characterises the simulation of the collision between
 37 light bullets and other sine-Gordon solutions and, finally, in section 4 the most important
 38 remarks are drawn.

39 2. Numerical method

In bidimensional cartesian coordinates, the (2+1)-dimension Klein-Gordon generalised
 equation becomes $\frac{\partial^2\phi}{\partial x^2} + \frac{\partial^2\phi}{\partial y^2} - \frac{1}{c^2} \frac{\partial^2\phi}{\partial t^2} = F(\phi)$. With the normalisation substitutions $x = \frac{\hbar}{mc}x'$, $y = \frac{\hbar}{mc}y'$ and $t = \frac{\hbar}{mc^2}t'$ and loosing the primes, the following equation results:

$$\frac{\partial^2\phi}{\partial x^2} + \frac{\partial^2\phi}{\partial y^2} - \frac{\partial^2\phi}{\partial t^2} = \left(\frac{\hbar}{mc}\right)^2 F(\phi) \quad (3)$$

40 In order to numerically solve (3), the finite differences method is implemented in *Math-*
 41 *ematica 5.0* ®. A rectangular domain $\{(t, x, y) : t \in [t_1, t_{n_t}] \wedge x \in [x_1, x_{n_x}] \wedge y \in [y_1, y_{n_y}]\}$ is
 42 chosen and an $n_t \cdot n_x \cdot n_y$ -point space-time grid is created with uniform steps $\Delta t = \frac{t_{n_t} - t_1}{n_t - 1}$,
 43 $\Delta x = \frac{x_{n_x} - x_1}{n_x - 1}$ and $\Delta y = \frac{y_{n_y} - y_1}{n_y - 1}$. Second-order derivatives are approximately computed
 44 through centered second-order differences.

45 Initial conditions are given by the definition of ϕ and $\frac{\partial\phi}{\partial t}$ at time t_1 . As for boundary
 46 conditions, for all simulations presented here fixed conditions are used along y -direction
 47 and periodic ones along x -direction.

48 One must take into account the convergence conditions of the method, $\frac{c^2\Delta t^2}{\Delta x^2} \leq \frac{1}{2}$ and
 49 $\frac{c^2\Delta t^2}{\Delta y^2} \leq \frac{1}{2}$, and, in the case of space-periodic solutions, the spatial grid's resolution has to
 50 be adequate: a solution with spatial periodicity through (a,b)-direction and with period

51 δ should be represented with some - say, 3 - points per period, that is, $\Gamma = \frac{\delta}{a\Delta x + b\Delta y} \geq 3$.
 52 Otherwise, meaningless results may be obtained.

53 The whole numerical approach refers to Klein-Gordon generalised equation. However,
 54 in this paper, only the sine-Gordon case is studied; thus, from now on $F(\phi) = \left(\frac{mc}{\hbar}\right)^2 \sin\phi$.
 55 Future developments may consider any other case using the same numerical method with
 56 the corresponding definition of F .

57 3. Results

58 3.1. Kink-like solitons

Theoretical approaches to (1+1)-dimension sine-Gordon equation [9,10] allow one to write an 1-soliton analytical solution in the (2+1)-dimension case as

$$\phi(t, \vec{r}) = 4 \operatorname{arctg} \left(\operatorname{Sign}(m) \cdot e^{\frac{\vec{d} \cdot (\vec{r} - \vec{r}_0) - \beta t}{\sqrt{1 - \beta^2}}} \right) \quad (4)$$

59 where $\beta = \frac{\sqrt{m^2 - 1}}{m}$, $|m| \geq 1$, \vec{d} is the normalised propagation direction and \vec{r}_0 the position
 60 of the center point at $t = 0$.

61 The case $m > 1$ corresponds to the so-called *kink*, an ascending step propagating
 62 along \vec{d} with velocity β . An example is presented on figure 1. Analogously, $m < -1$
 63 corresponds to an *antikink*, a descending step propagating along \vec{d} with velocity $-\beta$ (see
 64 figure 2). Both kink and antikink behave like solitons since they maintain their shape
 65 while propagating. Particular solutions are the cases $m = 1$ (*standing kink*) and $m = -1$
 66 (*standing antikink*) which are stationary.

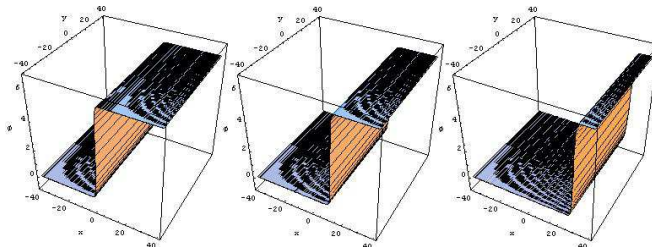


Fig. 1. Propagation of a kink with $m = 2$, $\vec{d} = \vec{e}_x$ and $\vec{r}_0 = \vec{0}$ within an $800 \cdot 401 \cdot 2$ -point grid defined in $\{(t, x, y) : t \in [0, 100] \wedge x \in [-40, 40] \wedge y \in [-40, 40]\}$. In the sequence of shots time flows from left to right.

67 3.1.1. Propagation

68 The dependence on the m parameter of the kink solution is studied. Regardless of
 69 the value of m , a nonlinear trail due to numerical reasons is always present in the
 70 propagation of the kink. As m rises, the trail becomes more significant, which may be
 71 explained by the steepening of the step. Indeed, $\phi \propto \operatorname{arctg} \left(e^{\frac{x}{\sqrt{1 - \beta^2}}} \right) = \operatorname{arctg} \left(e^{|m|x} \right)$
 72 $\left(\vec{d} = \vec{e}_x, \vec{r}_0 = \vec{0} \right)$. For $m = 7$ or higher, the kink is destabilised and no proper propagation

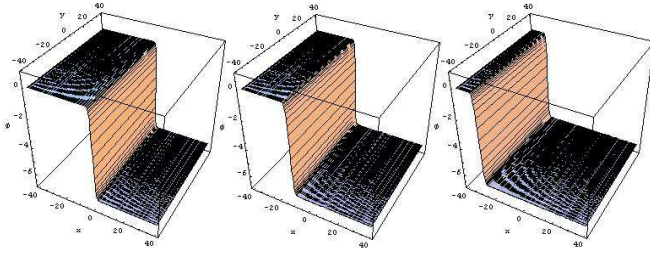


Fig. 2. Propagation of an antikink with $m = -2$, $\vec{d} = \vec{e}_x$ and $\vec{r}_0 = \vec{0}$ within an $800 \cdot 401 \cdot 2$ -point grid defined in $\{(t, x, y) : t \in [0, 100] \wedge x \in [-40, 40] \wedge y \in [-40, 40]\}$.

73 is achieved. Another important m -dependent feature is the propagation velocity. The
 74 theoretical motion is given by $x = x_0 + \beta t$ (if $\vec{d} = \vec{e}_x$); so, the velocity should be constant
 75 and equal to β . To determine this velocity numerically, several pairs of time and position
 76 of the center point are registered and a linear fit is applied using *Origin 5.0*® - an example
 77 is presented in figure 3. The results for $m = \{1.5, 2.0, 2.5, 3.0\}$ (using $\vec{d} = \vec{e}_x, \vec{r}_0 = \vec{0}$) are
 78 presented in table 1. It is obvious that greater values of m lead to less precision and
 79 exactness on the determination of the velocity. Taking into account the last column of
 80 table 1, the most favourable situation occurs when $m = 2.0$. Therefore, the next sections
 81 will use this kind of kinks (and the corresponding antikinks with $m = -2.0$) as they are
 82 less disturbed by numerical errors. Moreover, the fitted values of x_0 are close to 0, which
 83 means the law $x = x_0 + \beta ct$ is being followed ($\vec{r}_0 = \vec{0}$).

84 It is interesting to note that all velocities in table 1 are below 1 ($c = 1$), which is the
 85 typical velocity of a wave in the case $F(\phi) = 0$. As $m \rightarrow \infty$, the velocity of the kink
 86 tends to 1 since $\beta \rightarrow 1$.

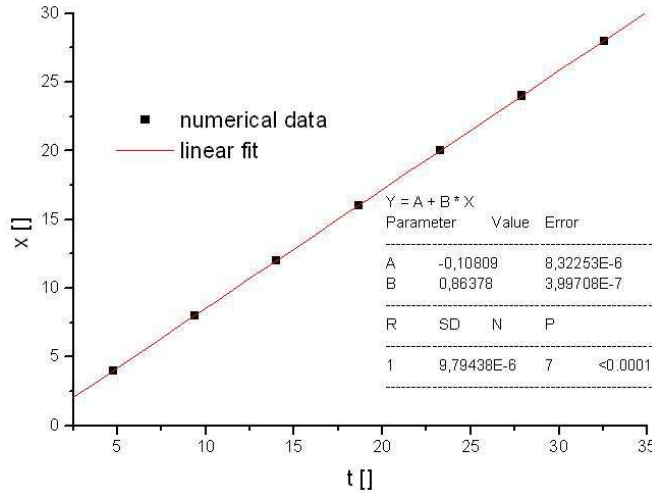


Fig. 3. Linear fit of pairs $\{time, position\}$ of the center point of a kink with $m = 2$, $\vec{d} = \vec{e}_x$ and $\vec{r}_0 = \vec{0}$ propagating within an $800 \cdot 401 \cdot 2$ -point grid defined in $\{(t, x, y) : t \in [0, 100] \wedge x \in [-40, 40] \wedge y \in [-40, 40]\}$.

m	$x_0^{(num)}$	$\beta^{(num)}$	$\beta^{(teo)}$	δ_β [%]
1.5	-0.093 ± 0.000	0.743 ± 0.000	0.745	0.28
2.0	-0.108 ± 0.000	0.864 ± 0.000	0.866	0.26
2.5	-0.081 ± 0.028	0.908 ± 0.001	0.917	0.97
3.0	0.017 ± 0.039	0.922 ± 0.002	0.943	2.25

Table 1

Determination of the propagation velocity of kinks with $m = \{1.5, 2.0, 2.5, 3.0\}$, $\vec{d} = \vec{e}_x$ and $\vec{r}_0 = \vec{0}$ propagating within an $800 \cdot 401 \cdot 2$ -point grid defined in $\{(t, x, y) : t \in [0, 100] \wedge x \in [-40, 40] \wedge y \in [-40, 40]\}$. The last column shows the relative difference between $\beta^{(num)}$ and $\beta^{(teo)}$: $\delta_\beta = \frac{|\beta^{(num)} - \beta^{(teo)}|}{\beta^{(teo)}} \cdot 100$.

3.1.2. Collision

The collision between kink-like solitons is achieved by superposing them. However, in general, this procedure is not legitimate since the sine-Gordon equation (2) is nonlinear. The condition for the coexistence of a pair of legitimate kink-like solitons is

$$\sin(\phi_1 + \phi_2) = \sin\phi_1 + \sin\phi_2 \quad (5)$$

where ϕ_1 and ϕ_2 are solutions of (2). Thus, two kink-like solitons may be superposed if their steps are sufficiently separated, because in that case on each grid point one of the two solutions is a multiple of 2π , which means (5) is verified. In this way, the kink-kink collision, shown in figure 4, can be easily started and studied. Only the collision of kinks with symmetric velocity and same $|m|$ is simulated. Future works may take into account other situations.

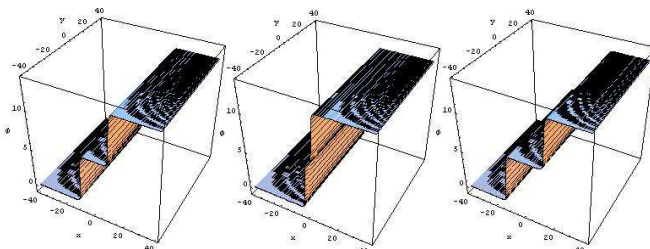


Fig. 4. Kink-kink collision. Both kinks have $m = 2$ and $\vec{d} = \vec{e}_x$; the kink propagating left-to-right (K \rightarrow) has $\vec{r}_0 = (-10, 0)$, while the one propagating right-to-left (K \leftarrow) has $\vec{r}_0 = (10, 0)$. An $800 \cdot 401 \cdot 2$ -point grid is defined in $\{(t, x, y) : t \in [0, 100] \wedge x \in [-40, 40] \wedge y \in [-40, 40]\}$.

Figure 4 shows that the kinks emerge intact (shape-wise) from collisions, which is typical of a soliton's behaviour. However, as they are nonlinear objects, they interact with each other during collisions. Evidence of this interaction is looked for in solitons velocity. The determination of the velocity follows the procedure explained in section 3.1.1, but picking pairs of time and position only after the interaction. The results obtained for each of the kinks are presented in table 2. Comparing these results with those referring to propagation only (table 1, line with $m = 2.0$), one understands that the value of β does not change significantly, while x_0 is now clearly above 0. This means that the interaction speeds up each one of the kinks, but does not alter their velocity afterwards.

	$x_0^{(num)}$ []	$\beta^{(num)}$ []
K→	0.703 ± 0.000	0.864 ± 0.000
K←	0.703 ± 0.000	0.864 ± 0.000

Table 2

Determination of the propagation velocity of the kinks in the kink-kink collision referenced by figure 4.

103 3.2. Light bullets

104 The *light bullet* [7,8] represents a well-localised two-dimensional moving pulse. Its pre-
105 viewed space-time dependence is

$$\phi(t, \vec{r}) = \sin\left(\gamma \vec{d} \cdot (\vec{r} - \vec{r}_0) + \omega t\right) \cdot e^{-\frac{1}{4\sigma^2} \left([\vec{d} \cdot (\vec{r} - \vec{r}_0)]^2 + [\vec{u} \cdot (\vec{r} - \vec{r}_0)]^2 \right)} \quad (6)$$

106 where $\omega = \sqrt{1 + \gamma^2}$ and \vec{u} is a normalised direction perpendicular to \vec{d} .

107 3.2.1. Propagation

The evolution of a single light bullet is represented in figure 5. There is no significant modification of shape - light bullets behave indeed as solitons. Nevertheless, a nonlinear trail is formed and the σ -value of the envelope function changes during propagation. To quantify the former, one compares the integral of ϕ in the trail region to that in the pulse region:

$$\epsilon = \frac{\int_{trail} \phi dx dy}{\int_{pulse} \phi dx dy}$$

The higher ϵ , the more important the trail is in comparison with the soliton. It is important to note that the trail is due not only to numerical reasons but also to the fact that (6) is not an analytical solution of (2), unlike the case of the kink-like solitons. The latter effect is evaluated fitting the numerical values of ϕ after propagation to

$$a_0 + a_1 e^{-\frac{1}{4a_2^2} \left([\vec{d} \cdot (\vec{r} - \vec{a}_3)]^2 + [\vec{u} \cdot (\vec{r} - \vec{a}_3)]^2 \right)}$$

108 where sometimes not all parameters are free to vary for convergence purposes.

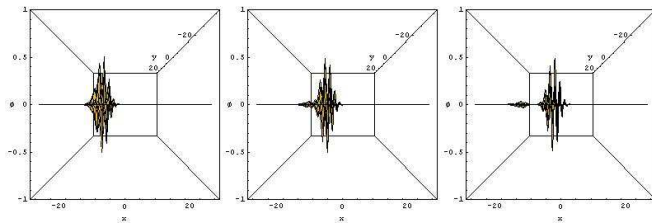


Fig. 5. Propagation of a light bullet with $\{\gamma, \sigma\} = \{2.0, 2.5\}$, $\vec{r}_0 = (-15, 0)$, $\vec{d} = \vec{e}_x$ and $\vec{u} = \vec{e}_y$. An $800 \cdot 151 \cdot 15$ -point grid is defined in $\{(t, x, y) : t \in [0, 100] \wedge x \in [-30, 30] \wedge y \in [-30, 30]\}$. The images are the projection of the solution in the xz plane. In this case, $\Gamma = 7.85$.

109 One can now study ϵ and a_2 as functions of γ and σ and then choose the most favourable
110 pair $\{\gamma, \sigma\}$ to perform collisions between light bullets. Tables 3 and 4 present the results
111 of these simulations. Although the case $\{\gamma, \sigma\} = \{1.0, 5.0\}$ is the one with less significant
112 trail, it leads to a strong deviation of σ after propagation. The pair of parameters $\{\gamma, \sigma\} =$
113 $\{2.0, 2.5\}$ seems to be the one in which less numerical errors occur; therefore, these are
114 the values used in the next sections.

$\sigma \setminus \gamma$	1.0	2.0	3.0
1.0	0.0402	0.0439	0.0447
2.5	0.0448	0.0430	0.0442
5.0	0.0380	0.0487	0.0461
Γ	15.71	7.85	5.23

Table 3

Values of ϵ for light bullets with $\gamma = \{1.0, 2.0, 3.0\}$ and $\sigma = \{1.0, 2.5, 5.0\}$ propagating within an $800 \cdot 151 \cdot 15$ -point grid defined in $\{(t, x, y) : t \in [0, 100] \wedge x \in [-30, 30] \wedge y \in [-30, 30]\}$. Γ -values are also shown for each γ used.

$\sigma \setminus \gamma$	1.0	2.0	3.0
1.0	2.688	1.156	2.067
2.5	2.704	2.468	2.573
5.0	5.907	4.596	4.639
Γ	15.71	7.85	5.23

Table 4

Values of the fitting parameter a_2 for light bullets with $\gamma = \{1.0, 2.0, 3.0\}$ and $\sigma = \{1.0, 2.5, 5.0\}$ propagating within an $800 \cdot 151 \cdot 15$ -point grid defined in $\{(t, x, y) : t \in [0, 100] \wedge x \in [-30, 30] \wedge y \in [-30, 30]\}$. Γ -values are also shown for each γ used.

115 3.2.2. Collision

116 Only the collision between light bullets of $\{\gamma, \sigma\} = \{2.0, 2.5\}$ is simulated. Other cases
117 may be dealt with in future approaches. The numerical method is started by superposing
118 light bullets according to (5). Figure 6 shows a head-on collision. The solitons interact
119 with each other and emerge essentially intact and with no change in propagation direc-
120 tion. However, the σ -value of the envelope function of each bullet does not behave as in
121 the propagation case. In fact, the value of the fitting parameter a_2 after collision is 2.09.
122 It seems that head-on collisions lead to a shrink of the soliton, but this conclusion must
123 be tested by further and more complete simulations.

124 3.3. Collision between light bullets and other solutions

125 In order to study the interaction of light bullets with kink-like solutions, kink-, antikink-
126 and standing kink-light bullet head-on collisions are set up and shown, respectively, in
127 figures 7, 8 and 9. In all three cases, the light bullet seems to emerge intact from the
128 interaction and continues its motion with no visible change. The velocities of the light

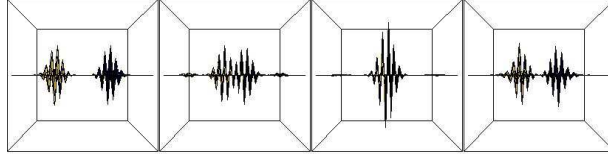


Fig. 6. Head-on collision between two light bullets with $\{\gamma, \sigma\} = \{2.0, 2.5\}$, $\vec{r}_{01} = (-15, 0)$ and $\vec{r}_{02} = (15, 0)$. An $800 \cdot 151 \cdot 15$ -point grid is defined in $\{(t, x, y) : t \in [0, 100] \wedge x \in [-30, 30] \wedge y \in [-30, 30]\}$. The images are the projection of the solution in the xz plane.

129 bullet in the propagation case (section 3.2.1) and in kink-light bullet head-on collision
 130 are roughly determined and no significant difference is noticed.

131 Moreover, a 30° -collision between a light bullet and a standing kink is simulated - see
 132 figure 10. As in the previous scenarios, no modification in the light bullet propagation
 133 direction is detected, which evidences the robustness of these objects.

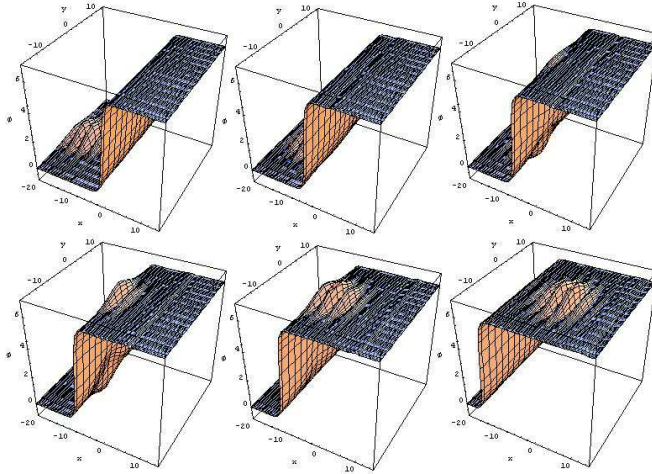


Fig. 7. Kink-light bullet head-on collision. The light bullet has $\{\gamma, \sigma\} = \{2.0, 2.5\}$, $\vec{r}_{01} = (-15, 0)$ and $\vec{d}_1 = \vec{e}_x$, while the kink presents $m = 2$, $\vec{r}_{02} = \vec{0}$ and $\vec{d}_2 = -\vec{e}_x$. An $800 \cdot 251 \cdot 31$ -point grid is defined in $\{(t, x, y) : t \in [0, 100] \wedge x \in [-30, 30] \wedge y \in [-35, 35]\}$ and this domain is zoomed into $\{(t, x, y) : t \in [0, 100] \wedge x \in [-20, 15] \wedge y \in [-15, 15]\}$. In the sequence of shots time flows from left to right and downwards. In this case, $\Gamma = 13.09$.

Another collision taken into account is the one between a light bullet and a *standing breather*, shown in figure 11. The latter object is an analytical solution of (2) which is oscillatory and may be interpreted as a bound state between a kink and an antikink. Its behaviour is previewed analytically in the (1+1)-dimension case [9] and can be extended to

$$\phi(t, \vec{r}) = 4 \operatorname{arctg} \left(\frac{m}{\sqrt{1-m^2}} \frac{\sin \omega t}{\cosh \left(m \vec{d} \cdot (\vec{r} - \vec{r}_0) \right)} \right) \quad (7)$$

134 where $\omega = \frac{2\pi}{T} = \sqrt{1-m^2}$ and $|m| < 1$. In this collision, the light bullet still emerges
 135 intact, although the standing breather is completely ruined after the interaction. In other

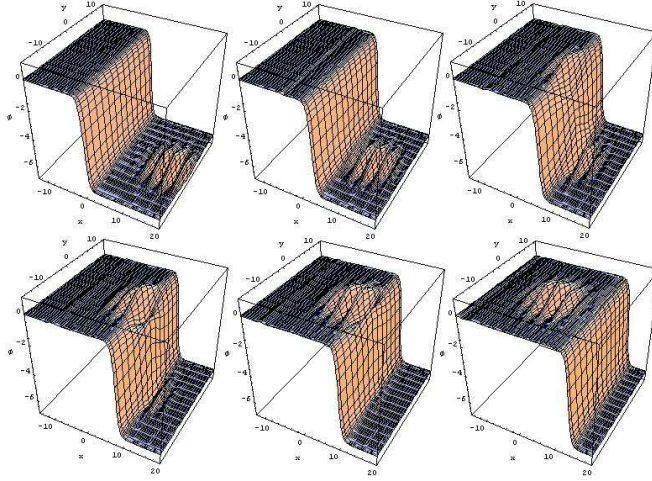


Fig. 8. Antikink-light bullet head-on collision. The light bullet has $\{\gamma, \sigma\} = \{2.0, 2.5\}$, $\vec{r}_{01} = (15, 0)$ and $\vec{d}_1 = -\vec{e}_x$, while the antikink presents $m = -2$, $\vec{r}_{02} = \vec{0}$ and $\vec{d}_2 = -\vec{e}_x$. An $800 \cdot 251 \cdot 31$ -point grid is defined in $\{(t, x, y) : t \in [0, 100] \wedge x \in [-30, 30] \wedge y \in [-35, 35]\}$ and this domain is zoomed into $\{(t, x, y) : t \in [0, 100] \wedge x \in [-15, 20] \wedge y \in [-15, 15]\}$. In this case, $\Gamma = 13.09$.

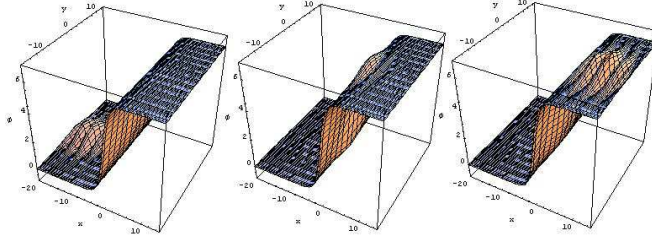


Fig. 9. Standing kink-light bullet head-on collision. The light bullet has $\{\gamma, \sigma\} = \{2.0, 2.5\}$, $\vec{r}_{01} = (-15, 0)$ and $\vec{d}_1 = \vec{e}_x$, while the standing kink ($m = 1$) presents $\vec{r}_{02} = \vec{0}$ and $\vec{d}_2 = \vec{e}_x$. An $800 \cdot 251 \cdot 31$ -point grid is defined in $\{(t, x, y) : t \in [0, 100] \wedge x \in [-30, 30] \wedge y \in [-35, 35]\}$ and this domain is zoomed into $\{(t, x, y) : t \in [0, 100] \wedge x \in [-20, 15] \wedge y \in [-15, 15]\}$. In this case, $\Gamma = 13.09$.

136 words, the bound state kink-antikink is destroyed by the light bullet, even though this
 137 does not destroy isolated kinks nor antikinks.

138 Figures 7, 8, 9, 10 and 11 all together allow one to confirm the robustness of light
 139 bullets observed in 3.2. Indeed, these solutions pass through analytical solutions (4) and
 140 (7) and remain unchanged. This property may have interesting consequences, specially
 141 if one identifies light bullets with optical pulses propagating in different media [8].

142 4. Final remarks

143 The analysis of kink and antikink solitons revealed an obvious shape consistency during
 144 propagation, which is typical of solitons behaviour. Moreover, an m -dependent study of
 145 the velocity in the kink case was carried out and it followed the theoretical solution (4),
 146 as expected.

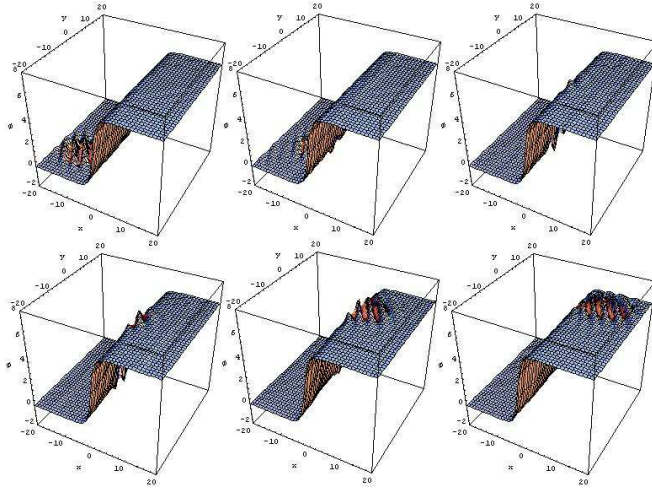


Fig. 10. Standing kink-light bullet 30° -collision. The light bullet has $\{\gamma, \sigma\} = \{2.0, 2.5\}$, $\vec{r}_{01} = (-15\cos 30^\circ, -15\sin 30^\circ)$ and $\vec{d}_1 = \cos 30^\circ \vec{e}_x + \sin 30^\circ \vec{e}_y$, while the standing kink ($m = 1$) presents $\vec{r}_{02} = \vec{0}$ and $\vec{d}_2 = \vec{e}_x$. An 800-61-61-point grid is defined in $\{(t, x, y) : t \in [0, 100] \wedge x \in [-30, 30] \wedge y \in [-30, 30]\}$ and this domain is zoomed into $\{(t, x, y) : t \in [0, 100] \wedge x \in [-20, 20] \wedge y \in [-20, 20]\}$. In this case, $\Gamma = 3.14$.

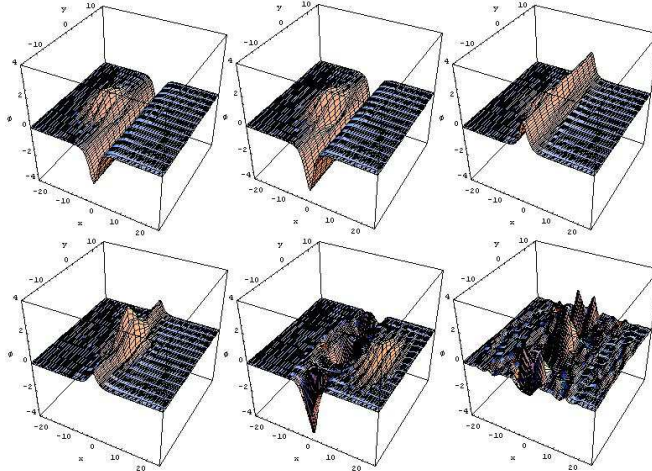


Fig. 11. Standing breather-light bullet head-on collision. The light bullet has $\{\gamma, \sigma\} = \{2.0, 2.5\}$, $\vec{r}_{01} = (-10, 0)$ and $\vec{d}_1 = \vec{e}_x$, while the standing breather presents $m = 0.8$, $\vec{r}_{02} = \vec{0}$ and $\vec{d}_2 = \vec{e}_x$. An $800 \cdot 251 \cdot 31$ -point grid is defined in $\{(t, x, y) : t \in [0, 100] \wedge x \in [-30, 30] \wedge y \in [-35, 35]\}$ and this domain is zoomed into $\{(t, x, y) : t \in [0, 100] \wedge x \in [-25, 25] \wedge y \in [-15, 15]\}$. In this case, $\Gamma = 13.09$.

147 As for kink-kink collision, one verified that kinks do not alter their shape, propagation
 148 direction nor velocity after head-on collisions with each other. Nevertheless, the numerical
 149 value of x_0 was found to be significantly above 0 for both kinks, which proves that
 150 nonlinear interaction has taken place and that it momentarily speeded up both solitons.

151 In the light bullet case, the propagation was characterised as a function of the param-
 152 eters γ and σ and the most favourable case was identified: $\{\gamma, \sigma\} = \{2.0, 2.5\}$. With this

153 configuration, a head-on collision was set up and nonlinear effects in the shape of the light
154 bullets were measured (through a_2). The shape consistency of the light bullets noticed in
155 the latter collision was also seen in head-on collisions with kink, antikink, standing kink
156 and standing breather.

157 Moreover, a 30° -collision between a light bullet and a standing kink was set up as
158 well and it reinforced the idea that light bullets and kinks are indeed robust objects. We
159 also found that the direction of the propagation of the light bullet is maintained after it
160 collides with the kink.

161 Future developments may study the dependence on γ and σ of light bullet collisions
162 and verify if these lead to a shrink of the light bullets or not. Another interesting point is
163 to understand why kink, antikink and standing kink survive to the collision with a light
164 bullet while the standing breather does not.

165

166 References

- 167 [1] *Solitons in the sine-Gordon equation*; Nonlinear Science; Los Alamos Science Special Issue 1987
168 [2] Di Garbo, A. et al; *Dynamical Properties of a Kink of the sine-Gordon Equation Trapped in a*
169 *Potential Well*; Nonlinear Analysis 47 (2001) 5967-5978
170 [3] <http://valdostamuseum.org/hamsmith/SnGdnPion.html>
171 [4] Sobolev, A., Pankratov, A. and Mygind, J.; *Numerical simulation of the self-pumped Long*
172 *Josephson junction using a modified Sine-Gordon model*; preprint submitted to Elsevier Science;
173 10th September 2005
174 [5] Wallraff, A., Ustinov, A., Kurin, V., Shereshevsky I. and Vdovicheva, N.; *Whispering Vortices*;
175 *Physical Review Letters*; volume 84; number 1; 3rd January 2000
176 [6] <http://homepages.tversu.ru/~s000154/collision/main.html>
177 [7] Povich, T. and Xin, J.; *A Numerical Study of the Light Bullet Interaction in the (2+1) Sine-Gordon*
178 *Equation*; *Journal of Nonlinear Science*; volume 15; 11-25; 2005
179 [8] Xin, J.; *Modeling light bullets with the two-dimensional sine-Gordon equation*; *Physica D* 135 (2000)
180 345-368
181 [9] Infeld, E. and Rowlands, G.; *Nonlinear waves, solitons and chaos*; Cambridge University Press;
182 1990
183 [10] Whitham, G.B.; *Linear and Nonlinear Waves*; John Wiley & Sons Inc; 1974